Effects of Different Gases on the Morphology of Ir Nanoparticles Supported on the TiO_2(110)-(1×2) Surface

A. Berkó and F. Solymosi*

Department of Solid State and Radiochemistry, University of Szeged, and Reaction Kinetics Research Group of the Hungarian Academy of Sciences, P.O. Box 168, H-6701 Szeged, Hungary

Received: June 7, 2000; In Final Form: September 7, 2000

The preparation of Ir nanoparticles supported on the TiO_2(110)-(1×2) surface and the effects of annealing in different gases were studied by scanning tunneling microscopy. The smallest Ir particles, measuring 1 nm and consisting of 8−10 atoms, were produced by the deposition of approximately 0.005 monolayer (ML) of Ir at 300 K. On an increase of the Ir coverage, the diameter of the particles gradually rose to 5 nm at 2 ML coverage. Annealing of the Ir-covered surfaces caused only slight changes below 700 K but led to migration and coalescence of the particles above 700 K. The hexagonal appearance of the larger particles suggested the formation of Ir crystallites with their (111) faces parallel to the plane of the support. The orientation of the slightly elongated particles was adjusted to the [001] direction of the TiO_2(110)-(1×2) surface. In the presence of CO (10^{-3} mbar), the smallest Ir particles (consisting of 8−10 atoms) disrupted into atomically dispersed Ir within a few minutes at 300 K. On an increase of the particle size, the disintegration proceeded more slowly, even at higher CO pressure. For particles larger than 3−4 nm, only minor corrosion of the nanoclusters was observed, even in the presence of 10 mbar CO. At higher temperature (600 K), the reversed process, the CO-induced agglomeration of small Ir particles, occurred. The adsorption of NO and O_2 also caused disruption of the Ir nanoparticles at 300−500 K. Such an effect was not experienced in the presence of N_2, which interacts only weakly with Ir_x crystallites.

1. Introduction

It has been demonstrated in a number of cases that the activity and selectivity of supported transition metal catalysts depend sensitively on the morphology (size and shape) of the metal particles.[1] Additionally, interactions between metal particles and the support may also influence the catalytic properties of the metals.[2−4] For this reason, characterization of such metal particles and evaluation of the possible interactions at metal/support interfaces are important tasks of catalysis research. A complicating factor is that the structures and sizes of metal particles are dramatically altered on contact with reacting gases, and a knowledge of these phenomena is therefore vital for an understanding of the catalytic reaction. The adsorption of CO on supported Rh provides a good example. Depending on the temperature, CO induces the disruption or agglomeration of Rh nanoparticles.[5−13] Several methods have been used to follow these structural changes, and scanning tunneling microscopy (STM) furnished direct evidence and a deeper insight into this surface process.[14,15] It was found that, through variation of the Rh content and the annealing temperature, Rh nanoparticles with dimensions in the range 1−10 nm can be produced. Supported Rh nanoparticles measuring 1−2 nm were observed to undergo very rapid disintegration to atomically dispersed Rh at 300 K, even after exposure for only a few minutes to 10^{-1} mbar CO. For particle sizes of 3−4 nm, the CO-induced process became slower, and for larger Rh clusters (8−10 nm), it did not occur at all, even at higher CO pressure. Keeping the atomically dispersed Rh in CO above 500 K led to re-formation of Rh clusters, but larger ones. CO-induced agglomeration was also observed for larger Rh particles (5−6 nm) above 500 K. The adsorption of NO on Rh nanoparticles likewise resulted in the disruption of Rh_x crystallites at 300 K. This was not observed, however, in the presence of H_2 and CO_2, which was explained by the different nature of their interactions with Rh. Recent (SPA)-LEED studies revealed that CO causes the spreading of the Rh particles deposited on a thin Al_2O_3 film, resulting in an expansion of their surface area.[16]

In the present work, STM was used to characterize the morphology of Ir nanoparticles of various sizes deposited on TiO_2(110), and the effects of different gases on the structure and size of the Ir crystallites. Apart from a short preliminary report on the interaction of CO with Ir/TiO_2(110), STM has not previously been employed to investigate the adsorption-induced structural changes in supported Ir particles.[17]

Numerous detailed STM studies have been published on the surfaces of single-crystal TiO_2, which is one of the most important support materials.[18−27] However, metal/TiO_2 interfaces have been characterized by STM only in a few cases: Rh/TiO_2-(001),[28] Rh/TiO_2(110),[29,30] Cu/TiO_2(110),[31] Ir/TiO_2(110),[28] Pd/TiO_2(100)-(1×3),[34,35] Ag/TiO_2(110),[36] Pt/TiO_2(100),[37] V/TiO_2-(110),[38] Al/TiO_2(110),[39] and Na/TiO_2(110).[40] Earlier, the electron spectroscopic studies on these systems have revealed that the noble metals form 3D clusters (Volmer−Weber growth) on the support surface. This feature was explained by the low reactivities of these metals with surface oxygen.[41] Determination of the morphology and localization of the adparticles by means of STM provides information on (i) the support sites where the crystallization starts, (ii) the registry with the oxide support, and (iii) the effect of the support morphology on the shape of the particles formed.[29,30,33,34,38] Moreover, the kinetics of surface diffusion may be exploited to produce nanoparticles with

* Corresponding author. Fax: ++ 36 62 420 678. E-mail: fsolym@chem.u-szeged.hu.

10.1021/jp002065u CCC: $19.00
Published on Web 10/14/2000

predetermined distribution, size and form for further spectroscopic studies.[30,32]

2. Experimental Section

The experiments were performed in an UHV system equipped with an STM head (WA-Technology), a three-grid AES-LEED analyzer, a quadrupole mass spectrometer and an Ar^+ gun. An UHV compatible auxiliary chamber separated by a gate-valve served for dosing of the sample at higher pressures. An ultimate pressure of 1×10^{-9} mbar was attained in both chambers by an iongetter and a titanium sublimation pump.

The polished $TiO_2(110)$ sample was purchased from Crystal Tec. It was clipped on a Ta plate and mounted on a transferable sample cartridge. An ohmically heated tungsten filament positioned just below the Ta plate served for annealing of the probe. The temperature in the range 300−1200 K was checked by a thin chromel−alumel thermocouple attached to the side of the sample. An infrared thermometer was also applied from time to time for outside temperature control. The cleaning procedure of the $TiO_2(110)$ surface consisted of a few hours annealing at 800 K in UHV, some cycles of Ar^+ ion bombardment (10 min, 1 kV, 10^{-5} A cm^{-2}) at room temperature, and annealing at 1200 K for 10 min in order to produce a well-ordered (1×2) arrangement.[23] This procedure resulted also in some reduction of the bulk and it increased the conductivity of the probe sufficiently for STM measurements. To receive good quality large terraces with nearly perfect (1×2) overstructure, we applied successfully a few minutes of Ar^+ bombardment (1 keV, 10^{-6} A cm^{-2}) during annealing at 1200 K. The purity of the surface was checked by AES measurements.

Iridium was deposited by ohmic heating of a high-purity (99.995%) Ir filament at the distance of approximately 20 mm from the sample. The amount and the purity of the epitaxial Ir layer on the $TiO_2(110)$-(1×2) surface was checked by AES. The concentration of the deposited metal is given in monolayer equivalent (ML), which corresponds to 1.5×10^{15} cm^{-2}. The calibration was mainly based on the appearing volume of 3D iridium crystallites observed on STM images at around 1 ML of admetal annealed at 1200 K. This method was described earlier in detail for rhodium deposited onto the same surface.[29] The coverage of the metal was controlled by duration of the evaporation. The typical deposition rate was 0.1 ML min^{-1}.

STM imaging of the surface was performed by a chemically edged tungsten tip sharpened from time to time in situ by applying 5−10 V pulses or by using a continuous positive bias of 40−70 V at 100 nA tunneling current between the tip and the sample. A tunneling bias of +1.5 V and current of 0.2 nA were typically used for STM imaging. The 256×256 points of an image were collected within 1−3 min depending on the size of the crystallites. For a better visualization of the surface morphology, an "emboss" procedure of a commercial software package was applied, although in some cases the application of a simple linear grayscale representation proved to be a better method. The characteristic pictures shown in this work were chosen from a number of imagines recorded on different regions of the same sample. It is worth mentioning that the overall morphologies on a scale of 100 nm × 100 nm measured on different sample regions were quite similar in each case.

3. Results

3.1. Thermal Stability of Ultrathin Ir Layers Deposited on $TiO_2(110)$-(1×2). The characteristic STM images of the clean $TiO_2(110)$-(1×2) surface were presented in a previous paper.[17,23] The typical STM image of a 100 nm × 100 nm area depicted characteristic step lines in the [001], [$\bar{1}$13], and [1$\bar{1}$1] directions, and well-ordered terraces with an average size of 500 nm^2. In the subsequent measurements, the regions where the presence of [001]-oriented steps are determining were chosen tendentiously. This arrangement was easily recognizable, even when the terrace inner structure was strongly disturbed by different treatments. Magnified images clearly showed the terrace morphology: parallel rows separated by 1.35 nm run in the orientation of [001]. The total area of the terraces revealed a complete reconstruction into the 1×2 arrangement. The average corrugation in the direction perpendicular to the rows was 0.08 nm. The fine details of the row structure were recently discussed in several papers.[18−26,42−44] Basically, two different explanations were proposed for this superstructure: (i) the missing oxygen row model, where some relaxations can also be taken into account;[21,22] and (ii) added Ti_2O_3 rows, suggested first in ref 19 and supported by some recent publications.[23,26,42−44] The difference in chemical activity toward formic acid and acetic acid for the bulk-terminated (1×1) and (1×2) reconstructed $TiO_2(110)$ surfaces strongly suggests that the latter model is the correct interpretation.[26,43] Moreover, there are some indications that the phase transition $(1\times1) \rightarrow (1\times2)$ proceeds more easily if the subsurface region is sufficiently reduced.[23,43]

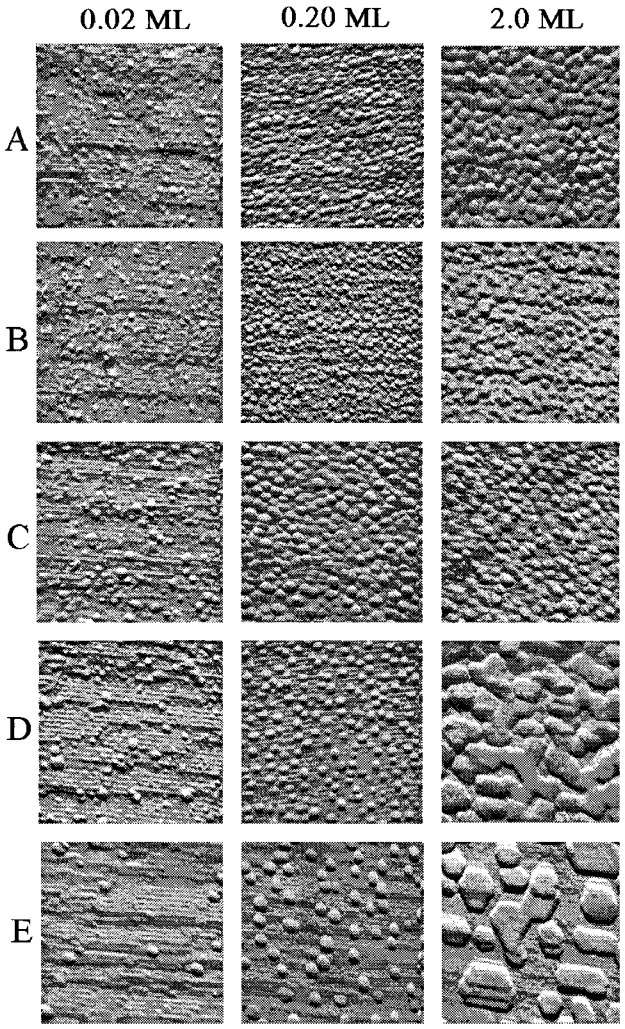

Figure 1. Effects of the deposition of Ir at (A) 300 K and after annealing in UHV for 10 min at different temperatures: (B) 500 K; (C) 700 K; (D) 900 K; (E) 1100 K. Image size: 50 nm × 50 nm. Figure reduced by 50% for publication.

Figure 1A presents STM images recorded after the deposition of different amounts of Ir onto the enhancement $TiO_2(110)$-

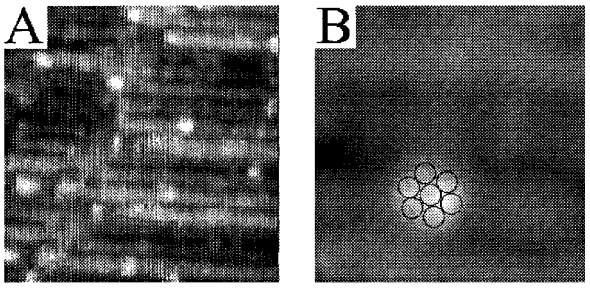

Figure 2. (A) Early stage of Ir_x particle formation for the coverage of <0.01 ML at room temperature. Image size: 20 nm × 20 nm. (B) An individual Ir particle consisting of few atoms imaged on 5 nm × 5 nm. Figure reduced by 40% for publication.

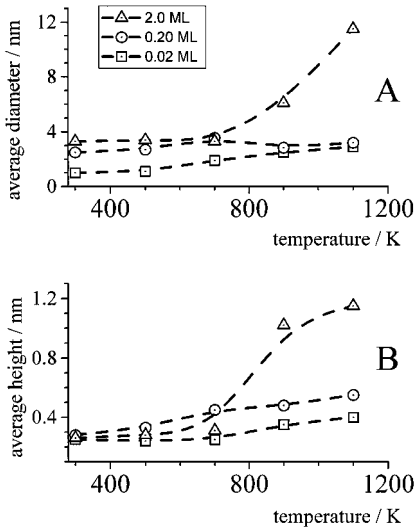

Figure 3. Changes in the average diameter (A) and the characteristic height of Ir particles (B) for three different initial coverages as a function of the annealing temperature.

(1×2) surface at room temperature. The average particle size increased with an increase of the Ir coverage: 1.5, 3.0, and 5.0 nm at 0.02, 0.20, and 2.0 ML, respectively. At the lowest coverage (0.02 ML), the original (1×2) arrangement of the support surface (step lines and terrace rows) can be clearly seen, together with many protrusions characteristic of the tiny admetal particles. The specific sites at which condensation of the admetal starts can be established on magnified images of the 0.005 ML Ir-covered surface (Figure 2A). Tiny Ir adparticles measuring 1 nm are located both on the terraces and at the step edges. Although the steps are not decorated preferentially, the outrising rows of the (1×2) terraces bind the Ir nanoparticles with high probability. The magnified image of a 5 nm × 5 nm area shows the localization of an individual Ir nanoparticle consisting of approximately 8−10 atoms (Figure 2B).

The effects of thermal treatment on the above Ir particles are shown in Figure 1B−E. Annealing at 500 K caused only slight changes in the surface morphology. A clear increase in the size of the particles occurred at 700 K, particularly for 0.02 and 0.2 ML of Ir. At 2.0 ML coverage, the particle size remained practically unaltered in this temperature regime. The average diameter and the height of the crystallites for different Ir coverages and annealing temperatures are depicted in Figure 3. At very low coverages (0.02 ML), annealing at 900−1100 K resulted in Ir particles approximately 3 nm in diameter, preferentially located at the step edges and crosspoints of the different edges (Figure 1D,E). More dramatic increases in the diameter and the height of the particles were detected at 2.0 ML (Figure 1D). In this case, annealing at 1100 K resulted in

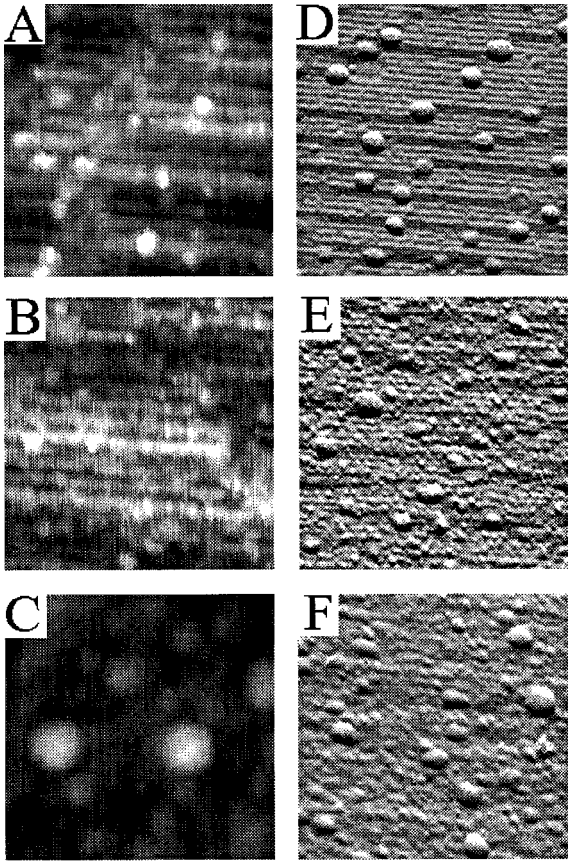

Figure 4. Effects of CO exposure on the STM images of Ir/TiO_2-(110)-(1×2): (A, D) before CO exposure; (B) after 10^{-3} mbar, 5 min, 300 K; (C) after 10^{-2} mbar, 10 min, 600 K; (E) after 10^{-1} mbar, 20 min, 300 K; (F) after 10^{-1} mbar, 20 min, 600 K. Image size: (A, B, C) 20 nm × 20 nm, (D, E, F) 50 nm × 50 nm. The original size of Ir nanoparticles: (A, B, C) 1.5 nm, (D, E, F) 3.0 nm. Figure reduced by 40% for publication.

hexagonal crystallites with the top (111) face parallel to the substrate (Figure 1E). One side of the hexagons was preferentially oriented in the close-packed [001] direction of the TiO_2-(110)-(1×2) surface. This behavior clearly pointed to crystallization coordinated by the row structure of the support. The larger particles were approximately 5−6 layer thick (1.0−1.2 nm), and their average diameter was 8−10 nm. Between the crystallites, the original (1×2) ordered terraces of the support were well detectable (Figure 1E). The fact that the probability of particle formation varied almost linearly with the Ir content provides a possibility of stimulating the concentration of crystallite seeds. The particles produced in this way can be selectively grown further by the evaporation of Ir at high temperature (1200 K).[32]

3.2. Effect of CO on the Morphology of the Supported Ir Particles. The effects of CO on the morphology of Ir crystallites were examined at different sizes. To obtain well-distinguishable particles, the Ir-containing samples were annealed at 400 K for a few minutes after evaporation. At the lowest Ir content (0.005 ML), the size of the Ir cluster was ∼1.0 nm. The tiny Ir particles (consisting of approximately 10 atoms) were located on the outrising rows of the substrate (Figure 4A). Exposure of this sample to CO (5 min, 10^{-3} mbar) at room temperature resulted in the disappearance of the larger clusters, in parallel with the appearance of tiny discontinuities on the originally flat rows (Figure 4B). It is worth mentioning that, to obtain a good-quality image, it was important to decrease the tunnel current (as low as 0.01 nA) after the exposure of CO, probably because of the

formation of weakly bonded carbonyl species. It may be noted that these images are original ones, without any further computational treatment. The structure and the size of the Ir particle formed as a result of CO adsorption changed radically when they were heated to 600 K in the presence of CO (10 min, 10^{-2} mbar) (Figure 4C). Although it is difficult to calculate exact total volumes because of tip convolution effects, it can be clearly stated that larger nanoparticles (approximately 3 nm) are formed.

Similar experiments were performed with Ir particles with an average diameter of 3−4 nm, grown by deposition of Ir (0.05 ML) at 300 K and annealing of the sample at 1100 K for 10 min. As shown in Figure 4D, approximately 20 particles are distributed on a surface area of 50 nm × 50 nm, which is the smallest representative region in this case. Most of the crystallites are bonded at the steps running in the [001] direction or at the crosspoints of different steps. Some of them, however, are localized in the middle of the reconstructed (1×2) terraces. The individual metal crystallites consist of approximately 200−300 atoms in this case. The rows of the substrate running in the [001] orientation are more or less continuous; merely a few discontinuities caused by contamination or defect sites can be seen. The exposure of this sample to CO (20 min, 10^{-1} mbar, 300 K) caused marked changes in the original texture of the surface (Figure 4E): (i) tiny dots measuring approximately 0.5 nm appeared, more or less uniformly distributed on the rows; (ii) although some larger particles (2−3 nm) could additionally be seen, their average size was definitely decreased; (iii) the top of the crystallites also displayed protrusions and the outline of the crystallites was strongly disturbed, though the imaging ability seemed rather good. A higher exposure of CO at room temperature did not cause any further change in the surface texture. When the above treated sample was heated to a higher temperature (600 K) in the presence of CO (10^{-1} mbar, 20 min), larger nanoparticles (4−5 nm) reappeared. At the same time, the interparticle region became covered by smaller crystallites (Figure 4F). By contrast, the same treatment of the clean TiO_2-(110)-(1×2) surface did not lead to structural changes.

It was described in section 3.1 that the deposition of 2.0 ML Ir onto TiO_2 at room temperature and annealing of the system for 10 min at 1100 K in UHV resulted in large hexagonal nanoparticles with an average diameter of 8−10 nm (Figure 5A). Exposure of this sample to 10^{-3} or 10^{-1} mbar CO at 300 K for 10 min caused only slight changes in the surface texture: small protrusions appeared both on top of the crystallites and on the terraces between the Ir particles (Figure 5B,C). The original particles were well detectable even after much higher CO exposure (10 mbar CO, 10 min) at slightly elevated temperature (400 K), although their shape was no longer well-defined, and new smaller crystallites (2−3 nm) appeared both on top of them and on the free terraces of the TiO_2 (Figure 5D). Such treatment did not cause any pronounced change in the overall corrugation ($\Delta z = 2.5$ nm) of the surface.

3.3. Effects of Other Gases: NO, O_2, and N_2. In the subsequent measurements, the effects of NO, O_2, and N_2 on the structure of Ir nanoparticles under the same experimental conditions were examined. Approximately 0.05 ML Ir was deposited on the TiO_2 support and annealed at 1100 K in UHV. The average diameter of the Ir particles was 3−4 nm, and the smallest characteristic region of 50 nm × 50 nm contained approximately 20 well-separated clusters (Figure 6A). Exposure of this surface to NO (10^{-1} mbar, 10 min) at room-temperature resulted in a definite decrease in the diameter of the Ir crystallites and in the appearance of smaller particles in the interparticle

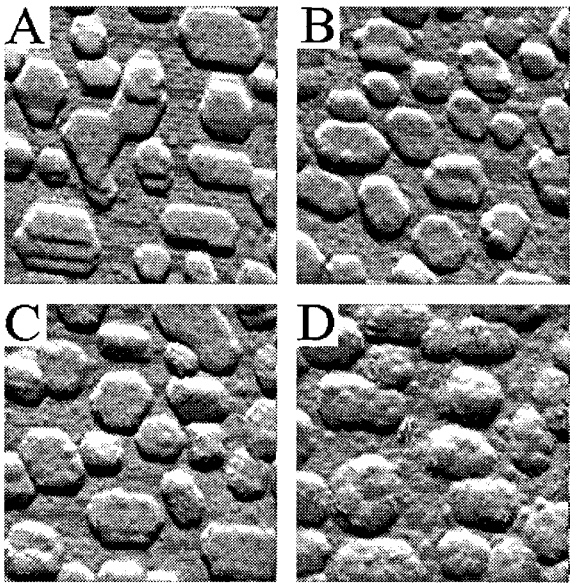

Figure 5. Effects of CO exposure on the shape of Ir nanoparticles of approximately 10 nm: (A) before CO treatment; (B) after gas adsorption 10^{-3} mbar, 300 K; (C) after 10^{-1} mbar, 300 K; (D) after 10 mbar, 400 K. Image size: 50 nm × 50 nm. Figure reduced by 40% for publication.

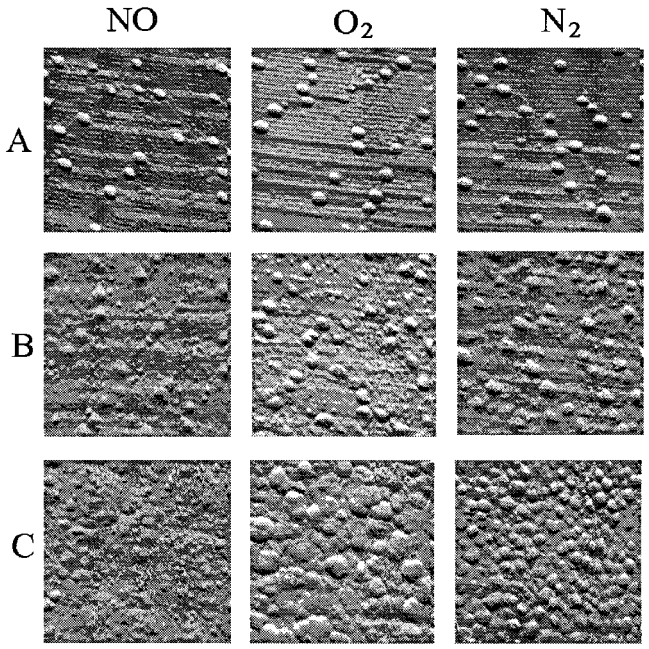

Figure 6. Effects of different gases (NO, O_2, N_2) on the STM images (50 nm × 50 nm) of Ir/TiO_2(110)-(1×2): (A) before gas exposure; (B) after gas adsorption, 10^{-1} mbar, 20 min, 300 K; (C) after 10^{-1} mbar, 20 min, 600 K. Figure reduced by 50% for publication.

regions (Figure 6B). In contrast, the adsorption of O_2 and N_2 led to much more moderate changes, although small protrusions occurred on the terraces of the TiO_2 (Figure 6B). Different features were observed at elevated temperature (600 K) (Figure 6C). NO adsorption led to a marked disintegration of the Ir particles, whereas O_2 increased the size of the particles considerably. In the presence of N_2, the average particle size did not change, but the particle-density definitely increased. This was a rather surprising but reproducible effect.

4. Discussion

4.1. Interaction of Ir with the TiO_2 (110)-(1×2) Surface. The behavior of ultrathin metal films grown on oxide surfaces is determined by the bond character between the metal atoms

and the substrate. The 3D Volmer−Weber growing mechanism predicts a rather weak interaction between the late transition metals (e.g., Pt and Rh) and the oxide surfaces with stoichiometric composition.[27,45] However, reducible surfaces or oxygen-deficient sites exhibit totally different features. One is the encapsulation of the admetal particles by suboxide species of the substrate at relative moderate temperatures.[37,46,47] Recent studies have shown that, although a measurable electron transfer can be excluded for stoichiometric TiO_2 surfaces, the weakly bonded electron localized on the oxygen-deficient (Ti^{3+}) sites is partly transferred to the transition metal adatom or cluster.[48,49]

STM is an especially informative method for the study of site-selective interactions between admetals and oxides. The results presented in this work clearly show that Ir atoms or tiny clusters consisting of less than 10 atoms are preferentially located at oxygen-deficient sites. If the added Ti_2O_3 row model is valid, it means that the formation of the Ir particles starts on the more reduced sites of the support, i.e., on the Ti_2O_3 rows. It is interesting that the bonding on these sites was only slightly preferred for Rh clusters of the same size.[29] This observation supports the experience that Ir can be produced in higher dispersity than Rh.[50] This trend is also valid for the Pd/TiO_2-(100)-(1×3) system, where no site preference was found on an atomic scale, and the formation of large particles at room temperature suggests a weaker wetting ability.[33] However, it may be noted that in a recent work, Xu et al. have found site-selective adsorption for Pd atoms.[34] Further low-temperature studies are needed to check the diffusion properties of transition metal atoms or small clusters on bulk-terminated and reconstructed TiO_2 surfaces.

The annealing of surfaces covered by far less than 1 ML of Rh or Ir resulted in crystallites measuring 1−3 nm localized preferentially at crosspoints of two differently oriented steps.[25,29] As these sites are probably oxygen-deficient, they bond the metal nanoparticles very strongly. This feature allows the selective growth of the crystallites bonded to the step crosspoints by further deposition of the metal at high temperatures.[30,32] At higher Ir coverages, the annealing resulted in agglomeration and collapse of the nanoparticles. The critical temperature proved to be 700−900 K: below this temperature, the Ir layer (or multilayer) efficiently wets the support; above it, the metal particles agglomerate into larger crystallites. This conclusion is more or less valid for the epitaxial Rh layer.[29] At the same time, it is rather surprising that nearly the same critical temperature (750 K) was found for Cu grown on the TiO_2(110)-(1×1) surface.[31] The melting points of Cu and Ir are very different: 1356 and 2683 K, respectively. This suggests that the accelerated mass transport found in all cases at about 800 K may reflect the diffusion properties of the support itself. It is well-known that the surface diffusion of Ti atoms on TiO_2(110) is activated at about 700 K.[51] Accordingly, this effect may contribute largely to an accelerated coalescence of the supported particles above 800 K.

The typical hexagonal shape of the crystallites formed clearly suggests the production of nanocrystallite slabs consisting of a few layers of (111) planes parallel to the plane of the support oxide surface and coordinated to the [001] orientation of the TiO_2(110)-(1×2) surface. Nearly the same behavior was found for epitaxially grown Rh on the same surface.[29] This feature can also be understood by taking into account the preferential (although less pronounced) bonding of Ir or Rh atoms to the more reduced Ti_2O_3 added rows.

4.2. Effects of Different Gases on the Structure of Supported Transition Metal Particles. It has long been recognized that the chemisorption of molecules can cause various changes in the state of metals, even in the case of single-crystal surfaces: (i) a change in the periodic relaxation of the layer−layer distance under the adlayer, extending for several layers in the bulk material; (ii) local or extended reconstruction of the outer metal layer; and (iii) selective surface segregation of one component of the alloy materials. As demonstrated in the present and previous studies, the effects of gas adsorption can be much more dramatic in the case of nanoparticles: it may lead to basic changes in the structures of metal crystallites.[5−17]

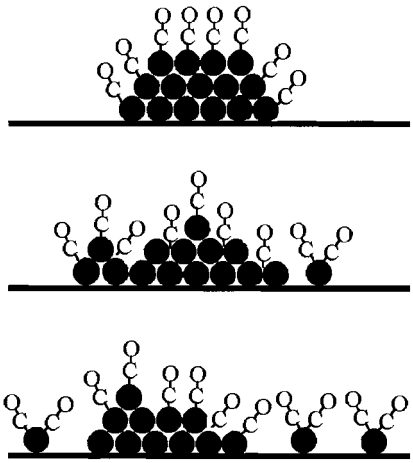

Figure 7. Model of the CO-induced disruption process.

In a study of the adsorption of CO on supported Ir by means of IR spectroscopy, we observed significant spectral changes at the time of the adsorption.[52] At the beginning of the adsorption at 300 K, a strong band appeared at 2060 cm^{-1}. This was attributed to the vibration of CO linearly bonded to Ir_x crystallites. With the progress of adsorption, however, two new bands developed, at 2010−2037 and 2090−2107 cm^{-1}; this was accompanied by attenuation of the band at 2060 cm^{-1}. These spectral features were tentatively assigned to the asymmetric and symmetric stretches of $Ir^+(CO)_2$ species. When a highly dispersed Ir sample was prepared, the adsorption of CO at room temperature yielded the dicarbonyl complex immediately, without the transient formation of Ir_x−CO. At lower temperature (150−200 K), however, the dominant form was still Ir_x−CO, and $Ir(CO)_2$ developed only by 270−300 K. On analogy with the well-studied CO−Rh system,[6,7] it was assumed that the state of Ir in the dicarbonyl species is an isolated Ir ion.[52] In the interpretation of these features, it was proposed that the adsorption of CO induced the disruption of Ir crystallites to give isolated Ir atoms, which were oxidized to Ir^+ by the OH groups of the support. Interestingly, the dicarbonyl species $Ir(CO)_2$ was transformed back into Ir_x−CO in the presence of CO above 423 K, suggesting the occurrence of the reductive agglomeration of isolated Ir^+ induced by CO.

The present STM studies provide direct evidence for the above processes and show that the adsorption-induced process is a size-dependent reaction. As illustrated in Figure 4, the small Ir crystallites (1−2 nm) are readily disrupted by CO adsorption, whereas such a process is much slower for particles measuring 3−4 nm or cannot be observed for Ir clusters larger than 8−10 nm. The driving force behind this process is very probably the higher Ir−CO bond energy of (159 kJ/mol) as compared to that of the Ir−Ir bond (146 kJ/mol); in other words, the formation of a strong Ir−CO bond results in rupture of the Ir−Ir bond.[53,54] The scheme presented in Figure 7 describes this morphological change.

The bonding of CO can be radically stronger on the different

surface sites, e.g., edges, kinks, or adatoms, sometimes even leading to dissociation of this molecule. We may assume that the species M−CO diffuses away from the remaining metal cluster, its diffusion occurring more easily than that of CO-free metals. This phenomenon may explain the gas-induced reduction in the activation energy of metal self-diffusion observed for many systems.[55]

The CO-induced agglomeration observed by means of IR spectroscopy at elevated temperatures (above 423 K) has been confirmed by the present STM measurements.[52] This was not restricted to isolated Ir atoms but occurred for larger Ir particles, too. We may assume that the transient formation of $Ir(CO)_2$ moieties contributes to the CO-promoted agglomeration of Ir clusters. This is followed by the diffusion of these species, which proceeds more easily than that of Ir metal particles, and then by the decomposition of $Ir(CO)_2$. As volatilization of Ir nanoparticles has never been observed in our experiments, we assume that the carbonyl species do not desorb into the gas phase. This mechanism can be referred to as gas-assisted Ostwald ripening, where larger islands grow as a result of dissolution of smaller ones.[56,57] Due to the change in the thermodynamic balance in the presence of a gas phase, the particle distribution shifts to a higher average particle size. It is important to note that the temperature at which agglomeration starts (approximately 500 K) is nearly the same as the temperature of CO desorption from extended Ir surfaces. In other words, the frequency of the adsorption−desorption processes is very high at around this temperature.

The disintegration of small Ir nanoparticles (3−4 nm) was also observed in the presence of NO, which was not revealed by IR spectroscopy, yet. The structural changes occurred more slowly as compared to the effect of CO but could be clearly demonstrated even at room temperature. In contrast with the effect of CO, the reverse process, the agglomeration of isolated Ir atoms, or of very small particles, did not proceed in the presence of NO at higher temperature. Moreover, the disintegration of undisrupted Ir particles further continued. This is consistent with the assumption that the adsorption-induced agglomeration of isolated Ir^+ is reductive in nature and cannot be initiated by NO. Although NO adsorbs less strongly than CO on Ir, its effect can be explained in the same way as for CO: the formation of a stronger Ir−NO bond leads to a weakening and finally to cleavage of the Ir−Ir bond. We may assume that NO likewise forms a surface complex, $Ir(NO)_2$, with isolated Ir atoms or ions, stabilizing the highly reactive Ir atoms or ions. In addition, it cannot be excluded that NO also oxidizes the most reactive Ir nanoparticles.

Exposure of $Ir/TiO_2(110)$ to N_2 at 300−500 K caused practically no change in the morphology and size of the Ir_x cluster, independently of the initial size of the Ir (Figure 6). This is in harmony with the above interpretation: the molecular N_2 interacts weakly with the Ir cluster at 300−500 K and cannot weaken or rupture the Ir−Ir bond. At the same time, the treatment in N_2 at 600 K induced reproducibly an increase of the surface concentration of the particles. To explain this feature, we may assume that the change in the morphology is caused by a strong roughening of the support under nonoxidative conditions. However, this phenomenon was not observed on the clean $TiO_2(110)$-(1×2) surface.

The effect of O_2 requires special discussion. On O_2 exposure, disruption of the nanoparticles proceeds below 400 K via the same mechanism as in the case of CO. Above 500 K, however, the small Ir particles may react with O_2, resulting in an increase in the average diameter of the oxidized Ir particles (Figure 6). This process was studied for supported Rh nanoparticles, and it was found that the onset temperature and pressure of formation of Rh_2O_3 are 500 K and 10^{-2} mbar O_2, respectively.[58]

5. Conclusions

(i) The deposition of Ir onto the $TiO_2(110)$-(1×2) surface at 300 K results in the growth of 3D clusters with an average diameter of 1−5 nm, depending on the admetal coverage. The smallest nanoparticles formed at approximately 0.005 ML coverage were bonded preferentially on the oxygen-deficient sites of the $TiO_2(110)$-(1×2) surface. (ii) Annealing of samples containing different amounts of Ir caused only moderate changes in morphology up to 700 K. The Ir nanoparticles formed at 1100 K are mainly hexagonal, suggesting development of the (111) plane of Ir crystallites oriented parallel to the support terraces with one side parallel to the [001] direction of the $TiO_2(110)$-(1×2) structure. (iii) Ir nanoparticles measuring 1 nm disrupted readily in the presence of 10^{-3} mbar CO at room temperature. With increase of the particle size, this process becomes slower, even at higher pressures. For particles measuring 8−10 nm, the use of 10 mbar CO and elevated temperature (400 K) is required to induce some corrosion at the perimeter of the nanoparticles. The reverse process (the agglomeration of smaller Ir particles) was observed in response to CO treatment at 600 K. (iv) NO and O_2 also caused disintegration of supported Ir nanoparticles below 500 K. In contrast, no disruption of Ir crystallites occurred in the presence of N_2.

Acknowledgment. This work was supported by the Hungarian Scientific Research Foundation Grant OTKA T-29952, T-32040.

References and Notes

(1) Boudart, M.; Djéga-Mariadassou, G. *Kinetics of Heterogeneous Catalytic Reactions*; Princeton University Press: Princeton, NJ, 1984.
(2) Solymosi, F. *Catal. Rev.* **1968**, *1*, 233.
(3) Schwab, G. M. *Adv. Catal.* **1978**, *27*, 1.
(4) *Metal support Interactions in Catalysis, Sintering and Redispersion*; Stevenson, S. A., Dumesic, J. A., Ruckenstein, E., Eds.; Van Nostrand Reinhold: New York, 1987.
(5) Van't Blik, H. F. J.; Van Zon, J. B. A. D.; Huizinga, T.; Vis, J. C.; Köningsberger, D. C.; Prins, R. J. *Am. Chem. Soc.* **1985**, *107*, 3139.
(6) Solymosi, F.; Pásztor, M. *J. Phys. Chem.* **1985**, *89*, 4783.
(7) Solymosi, F.; Pásztor, M. *J. Phys. Chem.* **1986**, *90*, 5312.
(8) Basu, P.; Panayotov, D.; Yates, J. T., Jr. *J. Phys. Chem.* **1987**, *91*, 3133.
(9) Buchanan, D. A.; Hernandez, M. E.; Solymosi, F.; White, J. M. *J. Catal.* **1990**, *125*, 456.
(10) Wong, T. T.; Stakheev, A. Yu.; Sachtler, W. H. *J. Phys. Chem.* **1992**, *96*, 7733.
(11) Evans, J.; Hayden, B.; Mosselmans, F.; Murray, A. *Surf. Sci.* **1992**, *279*, L159.
(12) Solymosi, F.; Knözinger, H. *J. Chem. Soc., Faraday Trans.* **1990**, *86*, 389.
(13) Solymosi, F.; Bánsági, T. *J. Phys. Chem.* **1993**, *97*, 10133 and references therein.
(14) Berkó, A.; Ménesi, G.; Solymosi, F. *J. Chem. Phys.* **1996**, *100*, 17732.
(15) Berkó, A.; Solymosi, F. *J. Catal.* **1999**, *183*, 91.
(16) Baumer, M.; Frank, M.; Libuda, J.; Stempel, S.; Freund, H.-J. *Surf. Sci.* **1997**, *391*, 204.
(17) Berkó, A.; Solymosi, F. *Surf. Sci.* **1998**, *411*, L900.
(18) Leibsle, F. M.; Murray, P. W.; Condon, N. G.; Thornton, G. *J. Phys. D−Appl. Phys.* **1997**, *30* (5), 741.
(19) Onishi, H.; Iwasawa, Y. *Surf. Sci.* **1994**, *313*, L783.
(20) Novak, D.; Garfunkel, E.; Gustafsson, T. *Phys. Rev. B* **1994**, *50* (7), 5000.
(21) Murray, P. W.; Condon, N. G.; Thornton, G. *Phys. Rev. B.* **1995**, *51* (16), 10989.
(22) Szabo, A.; Engel, T. *Surf. Sci.* **1995**, *329*, 241.
(23) Berkó, A.; Solymosi, F. *Langmuir* **1996**, *12*, 1257.
(24) Fischer, S.; Munz, A. W.; Schierbaum, K. D.; Göpel, W. *J. Vac. Sci. Technol. B* **1996**, *14* (2), 961.

(25) Murray, P. W.; Leibsle, F. M.; Muryn, C. A.; Fisher, H. J.; Flipse, C. F. J.; Thornton, G. *Surf. Sci.* **1994**, *321*, 217.
(26) Tanner, R. E.; Castell, M. R.; Briggs, G. A. D. *Surf. Sci.* **1998**, *412/413*, 672.
(27) Heinrich, V. E.; Cox, P. A. *The Surface Science of Metal Oxides*; University Press: Cambridge, U.K., 1994.
(28) Poirier, G. E.; Hance, B. K. J.; White, M. *J. Vac. Sci., Technol. B* **1992**, *10* (1), 6.
(29) Berkó, A.; Ménesi, G.; Solymosi, F. *Surf. Sci.* **1997**, *372*, 202.
(30) Berkó, A.; Solymosi, F. *Surf. Sci.* **1998**, *400*, 281.
(31) Caroll, D. L.; Wagner, M.; Ruhle, M.; Bonnell D. A. *J. Mater. Res.* **1997**, *12* (4), 975.
(32) Berkó, A.; Klivényi, G.; Solymosi, F. *J. Catal.* **1999**, *182*, 511.
(33) Murray, P. W.; Shen, J.; Condon, N. G.; Pang, S. J.; Thornton, G. *Surf. Sci.* **1997**, *380* (1), L455.
(34) Xu, C.; Lai, X.; Zajac, W.; Goodman, D. W. *Phys. Rev. B* **1997**, *56* (20), 13464.
(35) Stone, P.; Bennett, R. A.; Poulston, S.; Bowker, M. *Surf. Sci.* **1999**, *433*−*435*, 501.
(36) Martin, D.; Creuzet, F.; Jupille, J.; Borensztein, Y.; Gadenne, P. *Surf. Sci.* **1997**, *377* (1−3), 958.
(37) Gao, Y.; Liang, Y.; Chambers, S. A. *Surf. Sci.* **1996**, *365*, 638.
(38) Biener, J.; Wang, J.; Madix, R. J. *Surf. Sci.* **1999**, *442*, 47.
(39) Lai, X.; Xu, C.; Goodman, D. W. *J. Vac. Sci. Technol. A* **1998**, *16* (4), 2562.
(40) Murray, P. W.; Condon, N. G.; Thornton, G. *Surf. Sci.* **1995**, *323*, L281.
(41) Diebold, U.; Pan, J. M.; Madey T. E. *Phys. Rev. B* **1993**, *47*, 3868.
(42) Guo, Q.; Cocks, I.; Williams, E. M. *Phys. Rev. Lett.* **1996**, *77* (18), 3851.
(43) Cocks, I. D.; Guo, Q.; Patel, R.; Williams, E. M.; Roman, E.; Desegovia, J. L. *Surf. Sci.* **1997**, *377* (1−3), 135.
(44) Onishi, H.; Iwasawa, Y. *Phys Rev. Lett.* **1996**, *76*, 791.
(45) Campbell, C. T. *Surf. Sci. Rep.* **1997**, *27* (1−3), 1.
(46) Pesty, F.; Steinrück, H.-P.; Madey T. E. *Surf. Sci.* **1995**, *339*, 83.
(47) Berkó, A.; Ulrych, I.; Prince, K. C. *J. Phys. Chem. B* **1998**, *102*, 3379.
(48) Wei-Xing, X.; Schierbaum, K. D.; Goepel, W. *J. Solid State Chem.* **1995**, *119*, 237.
(49) Schierbaum, K. D.; Fischer, S.; Wincott, P.; Hardman, P.; Dhanak, V.; Jones, G.; Thornton, H. *Surf. Sci.* **1997**, *391*, 196.
(50) Solymosi, F.; Raskó, J. *J. Catal.* **1980**, *62*, 253.
(51) Grossmann, B.; Piercy, P. *Phys. Rev. Lett.* **1995**, *74* (22), 4487.
(52) Solymosi, F.; Novák, É.; Molnár, Á. *J. Phys. Chem.* **1999**, *94* (18), 7251.
(53) Zhdanov, V. P. *Surf. Sci.* **1984**, *137*, 515.
(54) Fu, T.-Y.; Tsong, T. T. *Surf. Sci.* **1999**, *421*, 157.
(55) Drechsler, M. *Surface Mobilities on Solid Materials*; Plenum Press: New York, 1983.
(56) Rainer, D. R.; Xu, C.; Goodman D. W. *J. Mol. Catal. A* **1997**, *119*, 307.
(57) Rosenfeld, G. R.; Morgenstern, K.; Beckmann, J.; Wulfhekel, W.; Laegsgaard, E.; Besenbacher, F.; Comsa, G. *Surf. Sci.* **1998**, *402*−*404*, 401.
(58) Kellogg, G. L. *Phys. Rev. Lett.* **1985**, *54* (1), 82.